J Mater Sci: Mater Med (2009) 20:2197–2205
DOI 10.1007/s10856-009-3788-z

Foam-like scaffolds for bone tissue engineering based on a novel couple of silicate-phosphate specular glasses: synthesis and properties

Chiara Vitale-Brovarone · Francesco Baino · Oana Bretcanu · Enrica Verné

Received: 2 February 2009 / Accepted: 19 May 2009 / Published online: 28 May 2009

Abstract Glass–ceramic scaffolds mimicking the structure of cancellous bone were produced via sponge replication technique by using a polyurethane foam as template and glass powder below 30 μm as inorganic phase. Specifically, a SiO_2-based glass of complex composition and its corresponding P_2O_5-based "specular" glass were used as materials for scaffolding. The polymeric sponge was thermally removed and the glass powders were sintered to obtain a replica of the template structure. The scaffolds were investigated and compared from a structural, morphological and mechanical viewpoint by assessing their crystalline phases, volumetric shrinkage, pores content and interconnection, mechanical strength. In addition, the scaffolds were soaked in acellular simulated body fluid to investigate their in vitro behaviour. The produced scaffolds have a great potential for bone reconstructive surgery because their features, such as shape, strength, bioactivity and bioresorption, can be easily tailored according to the end use.

1 Introduction

Since early 1970s, bioceramics have been widely investigated in orthopaedics, maxillo-facial surgery and dentistry for the substitution of small or extensive bone portions due to trauma, tumours removal, age-related diseases (osteoporosis, osteoarthritis) or other pathologies [1–3]. The use of alloplastic materials allows to overcome the main drawbacks of traditional autografts (low availability, risk of pain and death of healthy tissue at the donor site) and homografts (risk of disease transmission, need of immunosuppressant drugs for the patient) [4].

Hydroxyapatite (HA) has been traditionally proposed for hard-tissue repair because of its chemical and crystallographic similarity to the carbonated apatite in human bone and teeth [5]. Calcium phosphate (CaP) salts, such as β-tricalcium phosphate (β-TCP) or β-calcium pyrophosphate (β-CPP), can act as HA precursors and they have been usually adopted in dentistry [6, 7]. HA and CaP scaffolds exhibit an excellent biocompatibility but they are characterized by poor mechanical strength (below 1 MPa) [8, 9] in comparison with that of cancellous bone (2–12 MPa) [10, 11].

Bioactive glasses (BGs) and glass-ceramics (BGCs) have attracted the interests of many researchers because their properties can be tailored depending on glass composition. The word "bioactivity" was coined by Hench in 1971 when he and his colleagues synthesized Bioglass® [12]. Bioactivity denotes the ability to elicit a specific biological response at the interface of the material which results in formation of a bond between tissue and material [13–15]. BGs and BGCs contain silicon dioxide (SiO_2) as the network former and alkaline/alkaline-earthy metal oxides (Na_2O, K_2O and CaO) as network modifiers able to promote the sequence of reactions involved in the bioactive process when the implant is exposed to body fluids. The bonding of BGs has been attributed to the formation of a HA or apatite-like layer, similar to bone mineral, on the glass surface.

BGs and BGCs can be produced in two ways: (i) melt processing, followed by pouring into moulds or quenching into cold water to obtain a "frit", or (ii) sol–gel route. Hench demonstrated that melt-derived glasses can be bioactive

C. Vitale-Brovarone (✉) · F. Baino · O. Bretcanu · E. Verné
Materials Science and Chemical Engineering Department, Politecnico di Torino, Corso Duca degli Abruzzi 24, 10129 Torino, Italy
e-mail: chiara.vitale@polito.it

only if the silica content is less than 60 mol.% [13]. However, sol–gel glasses with up to 90 mol.% silica reveal a bioactive behaviour due to their high specific surface area, typically within 100–200 $m^2\ g^{-1}$, which promotes ion-exchange phenomena with biological fluids [16–18].

In the last decade, biocompatible degradable materials have attracted increasing interests in the field of tissue engineering. Calcium/phosphate-based glasses (CaP-Gs) offer a unique range of soluble materials whose degradation rate can be foreseen by tailoring the glass composition. CaP-Gs belong to the basic system P_2O_5–CaO–Na_2O, in which phosphorus pentoxide is the network former. It is possible to design the composition of CaP-Gs, according to the end use, by incorporating metal oxides, such as F_2O_3 [19], TiO_2 [20] and ZnO [21], at the expense of CaO and/or Na_2O. SiO_2 can be added to the composition because, disrupting the P_2O_5-based network, enhances glass solubility. CaP-Gs are degradable with resorption rate that matches bone healing and cells regeneration rate [22], and their products of degradation are tolerated by the body without the risk of inflammation [23]. In addition CaP-Gs, usually produced by a melting-quenching route, can be molten at low temperature if compared to silica-based glasses.

HA, CaP salts, BGs and CaP-Gs have been proposed and investigated as bone fillers in form of particulate and as materials for scaffolding. Scaffolds are usually 3-D porous templates aiming to temporarily repair or restore the body after disease or degeneration [24]. Scaffolds for bone tissue engineering should (i) be biocompatible, (ii) promote osteoblasts adhesion and activity stimulating osteogenesis, (iii) bond to the living bone creating a stable interface, (iv) possess mechanical properties (strength, stiffness) matching those of the surrounding bone and (v) be easily fabricated in a reproducible way to match the size and shape of bone defects.

The purpose of this study was the preparation and characterization of foam-like inorganic scaffolds for bone tissue engineering produced by using (i) a SiO_2-based glass and (ii) the corresponding P_2O_5-based "specular" glass. The scaffolds were fabricated by the sponge-replication technique [25–27]. The major novelty is that for the first time—in the authors' knowledge—scaffolds based on a couple of silicate/phosphate "specular" glasses were compared in detail as regards their structural, morphological and mechanical features and their in vitro behaviour.

Table 1 Composition of starting glasses

Glass	Composition (mol.%)					
	SiO_2	P_2O_5	CaO	Na_2O	MgO	K_2O
CEL2	45	3	26	15	7	4
ICEL2	3	45	26	15	7	4

2 Materials and methods

2.1 Synthesis of starting glasses

In this work, glass–ceramic scaffolds were produced by using two different "specular" glasses, hereafter named CEL2 and ICEL2. CEL2 was a silica-based glass belonging to the SiO_2–P_2O_5–CaO–MgO–Na_2O–K_2O system [28], whereas ICEL2 was a phosphate-based glass developed by modifying the chemical composition of CEL2 [29]. "Specular" glass means that the molar amounts of SiO_2 and P_2O_5 in the ICEL2 composition were inverted in comparison to those of CEL2 in order to prepare a phosphate glass with small silica content and without any variation of both the modifier oxides amounts and the former/modifier oxides molar ratio with respect to CEL2 composition. The complete molar compositions of these two glasses are listed in Table 1. Both glasses were prepared by melting the raw products in a platinum crucible in air; the synthesis details are summarized in Table 2. The molten glasses were poured on a preheated stainless steel plate; the materials were finally ground by ball milling and sieved to obtain powders below 30 μm.

2.2 Glasses characterization

The glass transition temperature (T_g), the crystallization temperatures (T_{XX}) and the melting temperatures (T_m) of CEL2 and ICEL2 were previously investigated by the authors [28, 29] by differential thermal analysis (DTA; DTA7 Perkin-Elmer; temperature range: 50–1200°C, heating rate: 20°C min^{-1}) and are listed in Table 3.

CEL2 and ICEL2 underwent wide-angle (2θ within 10–70°) X-ray diffraction analysis (XRD) using a X'Pert diffractometer (Bragg-Brentano camera geometry with Cu Kα incident radiation; working conditions: 40 kV, 30 mA).

Table 2 Preparation of starting glasses

Glass	Raw products	Melting conditions
CEL2	SiO_2, $Ca_3(PO_4)_2$, $CaCO_3$, Na_2CO_3, $4MgCO_3\ Mg(OH)_2 \cdot 5H_2O$, K_2CO_3	1400°C for 1 h (heating rate: 10°C min^{-1})
ICEL2	$(NH_4)_2HPO_4$, SiO_2, $Ca_3(PO_4)_2$, $Na_3PO_4 \cdot 12H_2O$, $Mg_3(PO_4)_2 \cdot 8H_2O$, K_2HPO_4	1200°C for 1 h (heating rate: 10°C min^{-1})

Table 3 Results of the thermal analysis carried out on CEL2 and ICEL2

Glass	T_g (°C)	T_{XX} (°C)	T_m (°C)
CEL2	550 ± 10	760 ± 10; 810 ± 10	1050 ± 15
ICEL2	410 ± 10	590 ± 10	660 ± 10; 675 ± 10

2.3 Scaffolds fabrication

The polymeric template chosen for scaffolds preparation was a commercial open-cells PU sponge (apparent density ~20 kg m^{-3}). The polymer was cut into 15.0 × 15.0 × 15.0 mm^3 cubic blocks and then impregnated with a water-based CEL2 or ICEL2 slurry. The weight composition of both slurries was the following: 30% glass, 64% distilled water and 6% polyvinyl alcohol (PVA), which was used as binding agent to optimize the ability of glass particles to uniformly coat the template. First PVA was hydrolyzed in water by continuous magnetic stirring at 60°C for 1 h and then the glass powders were dispersed in the solution; the water evaporated during PVA dissolution was re-added to the slurry. The sponge blocks were soaked into the glass slurry for 60 s, taken back and compressed (20 kPa for 1 s) in the three spatial directions aiming to remove the exceeding slurry. This infiltration-compression process was repeated for several times. Finally, the samples were dried at room temperature for 6 h and thermally treated in order to remove the organic phase and to sinter the inorganic one, thus obtaining macroporous glass-ceramic scaffolds. The thermal treatment was set at 1000°C/3 h for CEL2-derived scaffolds and at 610°C/3 h for ICEL2-derived scaffolds (heating rate: 5°C min^{-1} for both thermal treatments). The sintering conditions were chosen on the basis of thermal analysis data and hot stage microscopy results [27, 29] to attain a good samples densification coupled with the minimum shrinkage.

2.4 Scaffolds characterization

XRD analysis was performed on the ground scaffolds to detect the presence of crystalline phases after sintering.

Scaffolds structure and morphology were evaluated through scanning electron microscopy (SEM, Philips 525 M) to assess pores size, shape and distribution.

The volumetric shrinkage Σ_{vol} (%), due to the PU template removal and to the glass softening-sintering, was estimated as

$$\Sigma_{vol} = \left(\frac{V_0 - V_s}{V_0}\right) \times 100,$$

where V_0 is the volume of the impregnated sponge before the thermal treatment and V_s is the scaffold volume.The porosity content $\prod$ (vol.%) was calculated, through geometrical mass–volume evaluations, as

$$\Pi = \left(\frac{\rho_g - \rho_s}{\rho_g}\right) \times 100,$$

where ρ_g is the density of non-porous glass and ρ_s is the apparent density of the scaffold (mass/volume ratio).

The presence of a 3-D network of interconnected pores was qualitatively assessed by means of capillarity tests. A face of the scaffold was put into contact with a thin film of calf serum, in which some drops of red ink were dispersed to simulate the colour of blood, to verify if the fluid was infiltrating the porous network due to capillarity forces.

The scaffolds strength was evaluated through crushing tests (MTS System Corp. apparatus, cross-head speed set at 1 mm min^{-1}); the failure stress σ_f (MPa) was obtained as

$$\sigma_f = \frac{F_M}{A_r},$$

where F_M (N) is the maximum compressive load registered during the test and A_r (mm^2) is the resistant area perpendicular to the load axis.

Finally, in vitro tests were carried out by soaking the scaffolds in acellular simulated body fluid (SBF), prepared according to Kokubo's protocol [30], that mimics the ion composition of human plasma. The samples were soaked for different time frames in 30 ml of SBF maintained at 37°C; the solution was replaced every 48 h to simulate fluid circulation in the human body. The pH variations induced by ion-exchange phenomena, were daily monitored (SBF reference value: pH = 7.40). After soaking, the samples were dried at room temperature and then investigated through SEM equipped with EDS system (Philips Edax 9100) for compositional analysis. A quantitative evaluation of phosphate scaffolds solubility was attained by weighting the samples before and after soaking and by then calculating the weight loss.

3 Results and discussion

3.1 Starting glasses

CEL2 showed two crystallization temperatures but only one melting temperature, because the two crystalline phases melted simultaneously. On the contrary, ICEL2 exhibited one T_{XX} value but two T_m values: in this case, the crystalline phases nucleated at the same temperature.

XRD spectra of as-poured CEL2 and ICEL2, reported in Fig. 1 and show only a broad halo revealing that the starting materials did not contain crystalline phases and are completely amorphous glasses.

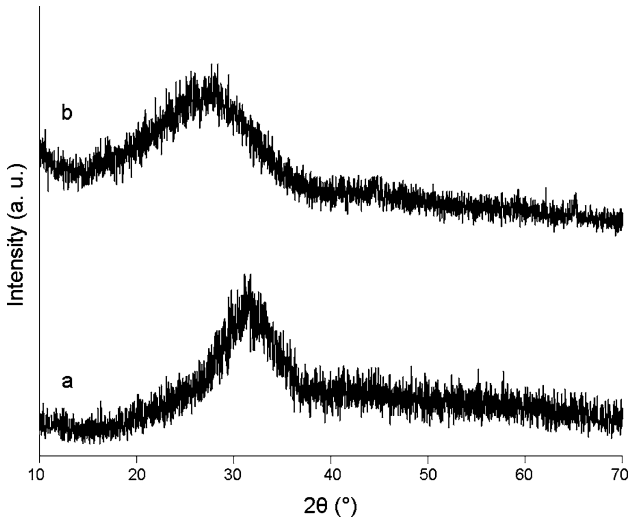

Fig. 1 XRD patterns of as-poured glasses: (a) CEL2 and (b) ICEL2

3.2 Scaffolds structural and morphological characterization

Figure 2 depicts the structure of the PU sponge, used as scaffolds template, that exhibits a 3-D network of pores ranging from 200 up to 800 μm with trabeculae thickness within 10–50 μm. The porosity of the sponge, assessed by weight-volume measurements, was ~95 vol.%. The polymeric skeleton was coated with a thin and continuous layer of glass particles (Fig. 3) in order to obtain, after the organic phase removal, an inorganic CEL2-derived or ICEL2-derived replica of the template.

After sintering, the resulting scaffolds were glass-ceramic because the thermal treatment induced the nucleation of crystalline phases from the glass amorphous phase, as detected by XRD investigations (Fig. 4). Specifically, in good accordance with previous work [27, 29], the crystalline phases were indexed as $Na_4Ca_4(Si_6O_{18})$ (combeite) and $Ca_2Mg(Si_2O_7)$ (akemanite) for glass-ceramic CEL2 (GC-CEL2), and as $Na_2Mg(PO_3)_4$ and $Ca_2P_2O_7$ (calcium pyrophosphate) for glass–ceramic ICEL2 (GC-ICEL2). It is worth to underline that these phases are well known to be highly biocompatible [31, 32]. Concerning GC-CEL2, it was demonstrated by other authors that crystals of combeite promoted material bioactivity [33] and a combeite-like phase was also found in sintered Bioglass®, which has been in clinical use since 1993 as Perioglas®, used to fill periodontal defects, and as NovaBone®, used in orthopaedic applications. [12]. As regards GC-ICEL2, calcium pyrophosphate is known to act as precursor of HA or apatite-like phases mimicking bone mineral [34–36].

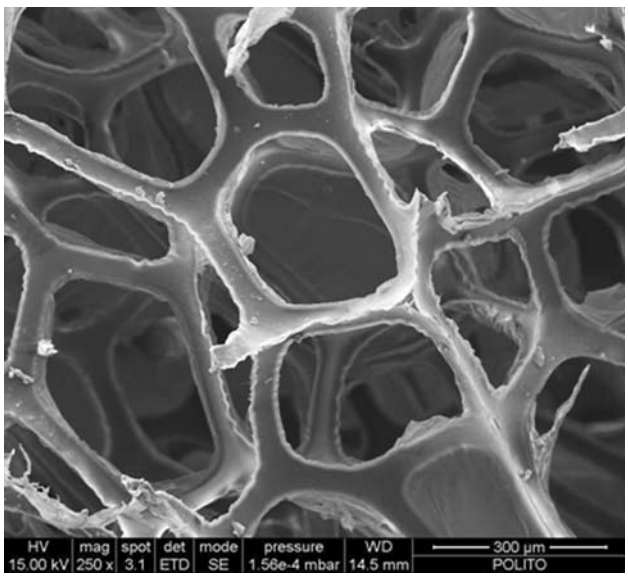

Fig. 2 Bare polymeric template

The presence of two crystalline phases in both GC-CEL2 and GC-ICEL2 scaffolds is consistent with thermal analysis data (Table 3). In fact, the crystalline phases assessed by XRD investigations have an actual correspondence with the crystallization/melting temperatures found via DTA.

The produced cubic scaffolds are shown in Fig. 5a–b: the high porosity of the samples is already evident from these low-magnification pictures. The grey colour of GC-ICEL2 scaffolds is due to presence of negligible amount of carbon residual of the PU template due to the low sintering temperature. It should be noticed that the sponge replication method involves a great potential for scaffolds fabrication, because the easiness of shaping the starting polymeric template allows to produce implants matching the bone defects and tailored to each single patient.

The effective densification of the pores struts, detected for both scaffolds, demonstrates that a good degree of sintering was achieved, as shown in Figs. 6 and 7. It should be noticed that a higher degree of sintering was obtained for GC-CEL2 scaffolds (Fig. 6) in comparison with GC-ICEL2 scaffolds (Fig. 7). The obtained 3-D network of open and interconnected macropores, ranging within 100–500 μm, closely mimics the trabecular morphology of natural cancellous bone. In addition, a high interconnection of the macropores plays a key role to promote the fast in vivo vascularization of the implant [15].

The volumetric shrinkage of the scaffolds due to sintering is reported in Table 4. It is a crucial parameter for scaffold design and preparation as it allows to tailor the final scaffold in terms of size and shape in order to fabricate "patient-designed" grafts. The porosity $\prod$ reported in Table 4 is the scaffolds whole pores content including the contribution of both macro- (>100 μm) and micropores (<100 μm).

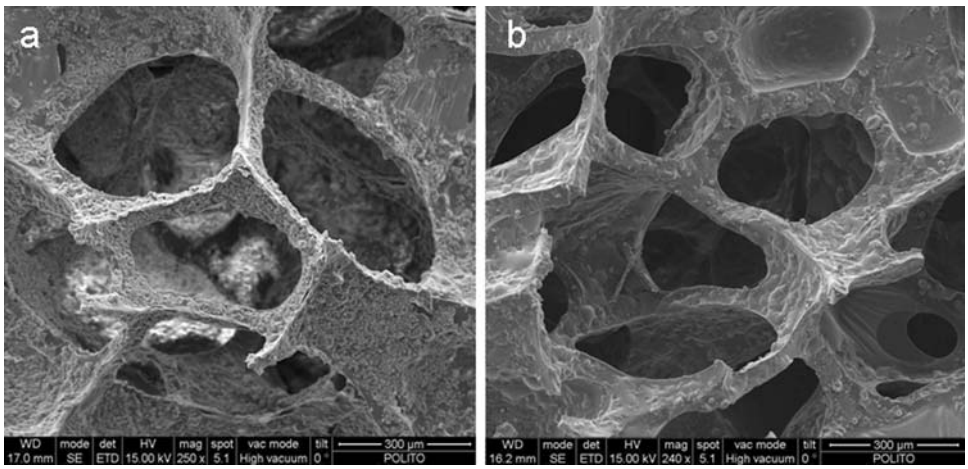

Fig. 3 Impregnated sponge: **a** CEL2-coated and **b** ICEL2-coated polymer

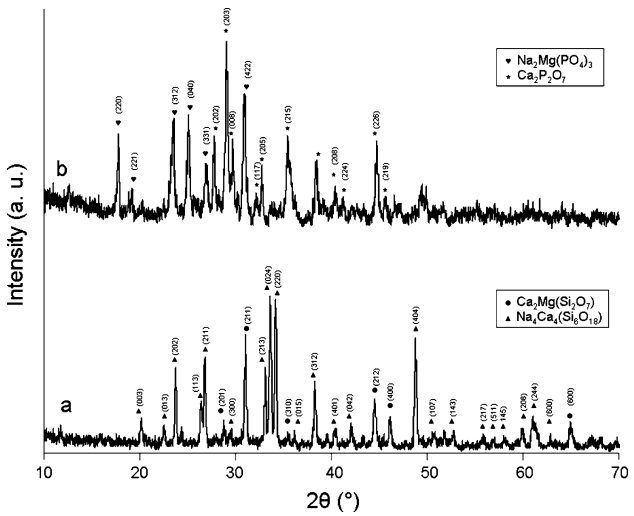

Fig. 4 XRD patterns of (a) GC-CEL2 scaffold and (b) GC-ICEL2 scaffold

The low standard deviation found for the volumetric shrinkage and pores content assesses the reproducibility of the prepared samples.

The sequence of pictures shown in Fig. 8a–e depicts the phases of the capillarity test performed on a GC-ICEL2 scaffold. The calf serum went up through scaffold pores network in a couple of seconds; similar results were obtained for GC-CEL2 scaffolds. In Fig. 8f the cross-sections of a GC-CEL2 scaffold before and after the test are compared: the presence of the red fluid in the inner part of the scaffold further confirms the high interconnection degree of the porous texture.

3.3 Scaffolds mechanical testing

Figure 9 reports two examples of GC-CEL2 and GC-ICEL2 scaffolds stress–strain (σ–ε) curves. Both scaffolds exhibited, as foreseen, a failure mode typical for brittle ceramics, i.e. the catastrophic failure after the maximum stress. The jagged profile of the curves is due to the progressive cracking of scaffolds trabeculae. As regards GC-CEL2 scaffold, the first peak visible in Fig. 9a can be attributed to the fracture of thinner trabeculae, whereas the second peak corresponds to the crumbling of thicker trabeculae, according to a mechanism described elsewhere [36, 37].

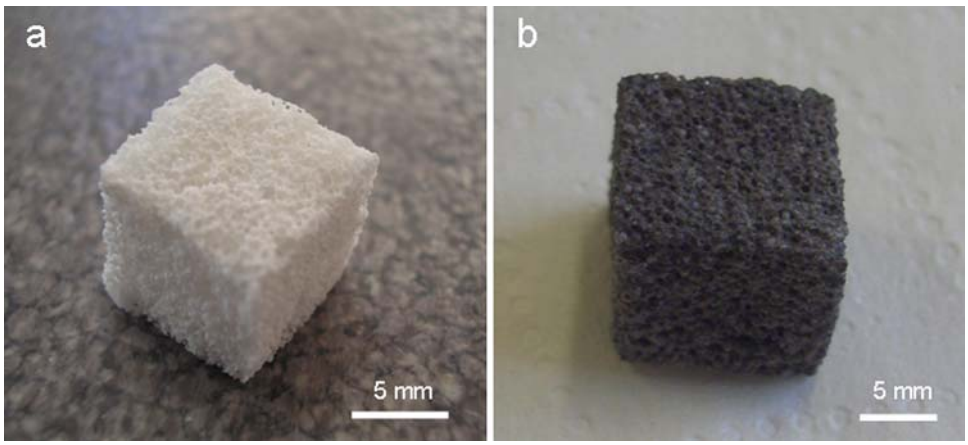

Fig. 5 (**a**) GC-CEL2 scaffold and (**b**) GC-ICEL2 scaffold

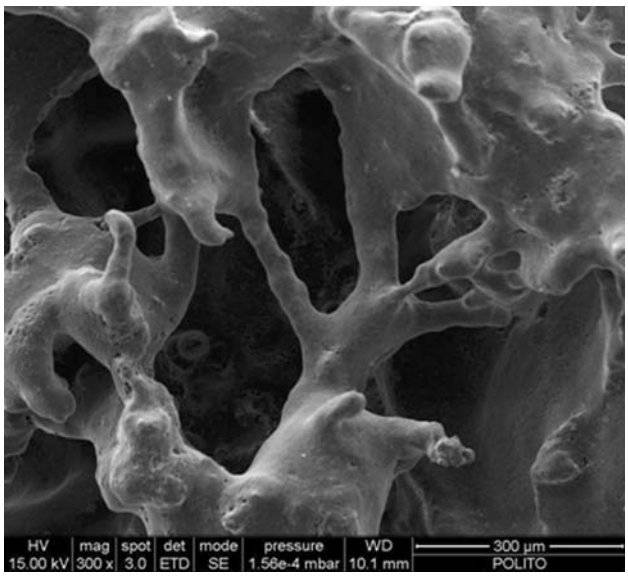

Fig. 6 SEM micrography of GC-CEL2 scaffold

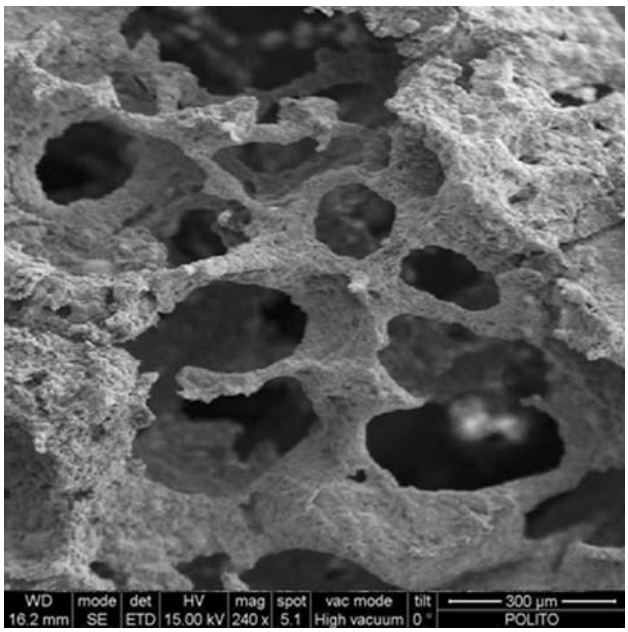

Fig. 7 SEM micrography of GC-ICEL2 scaffold

Table 4 Features of the produced scaffolds

Scaffold material	Σ_{vol} (%)	$\prod$ (vol.%)
GC-CEL2	64.5 ± 2.0	54.8 ± 4.5
GC-ICEL2	47.1 ± 3.0	82.0 ± 6.7

Five scaffolds tested for each series

The failure stresses are reported in Table 5. The compressive strength of GC-CEL2 scaffolds is one order of magnitude higher than that of GC-ICEL2 scaffolds: this can be attributed both to the different pores content, which was higher in GC-ICEL2 scaffolds than in GC-CEL2 ones (Table 4), and to the intrinsic mechanical properties of GC-CEL2 and GC-ICEL2. In addition, as shown in Figs. 6 and 7, a higher degree of sintering was achieved for GC-CEL2 scaffolds with respect to GC-ICEL2 ones; therefore, the trabeculae of the silicate scaffolds were sounder than those of the phosphate ones.

GC-CEL2 scaffolds were very promising candidates for bone grafting as they closely match the pores content and mechanical strength of cancellous bone [10, 11]. On the contrary, the strength of GC-ICEL2 scaffolds, although being comparable to today's commercially available ceramic (glass) scaffolds such as Bioglass®-derived scaffolds [38], is still unsatisfactory for load-bearing implants.

3.4 Scaffolds in vitro behaviour

GC-CEL2 and GC-ICEL2 scaffolds exhibited a different in vitro behaviour due to the peculiar properties of the starting glasses composition.

Figure 10a shows a GC-CEL2 scaffold cross-section after soaking for 7 days in SBF; the sample was embedded in epoxy resin (Struers), cut by means of a diamond rotating wheel and finally polished by SiC grit papers. A thick layer (20–80 µm) of a newly formed phase grown on pores walls is clearly distinguishable. EDS investigations (Fig. 10b) revealed that this layer was composed by only calcium and phosphorus with Ca/P molar ratio of 1.66, that closely approaches the Ca/P value of natural HA (1.67). The XRD pattern, shown in Fig. 11, revealed several marked peaks that can be actually indexed as the main reflections of HA phase, in accordance with EDS results. The two main peaks are broad due to the micro-crystalline nature of HA grown on bioactive glasses [39]. Therefore, GC-CEL2 scaffolds are expected to stimulate in vivo cells colonization and osteogenesis, as a HA layer promotes osteoblasts adhesion on scaffolds walls [40].

Figure 12 shows GC-ICEL2 scaffold structure after soaking for 1 month in SBF: scaffold struts became thinner and pores size increased because, as expected, the phosphate scaffold underwent an erosion process. The weight losses were 8.0 ± 2.0%, 12.0 ± 2.7% and 17.0 ± 3.1%, respectively, after soaking for 7, 30 and 90 days in SBF.

The pH variations in the solution were quite moderate for both scaffolds (pH within 7.30–7.55); therefore, no cytotoxic effect is foreseen after in vivo scaffolds implantation.

4 Conclusions

In this work, two kinds of macroporous foam-like glass-ceramic scaffolds, based on a couple of silicate-phosphate

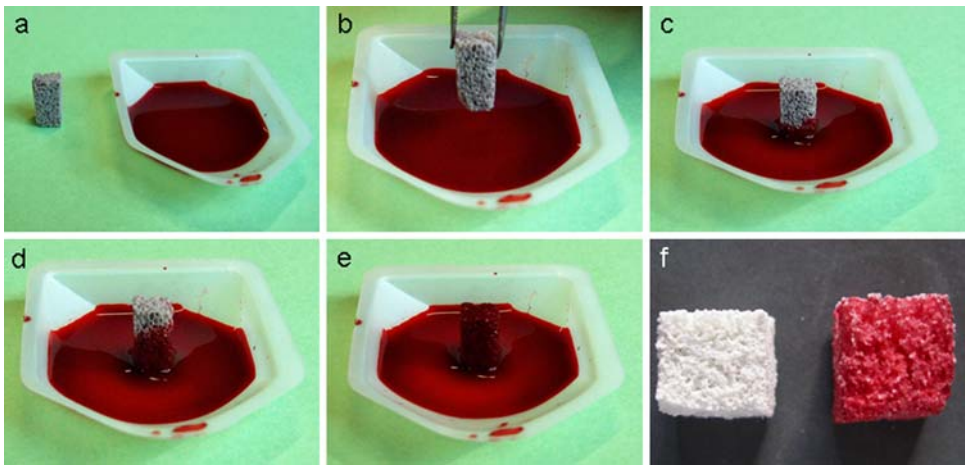

Fig. 8 Capillarity test: (**a**–**e**) phases of the test carried out on GC-ICEL2 scaffold, (**f**) comparison between the cross-sections of GC-CEL2 scaffold before and after the test

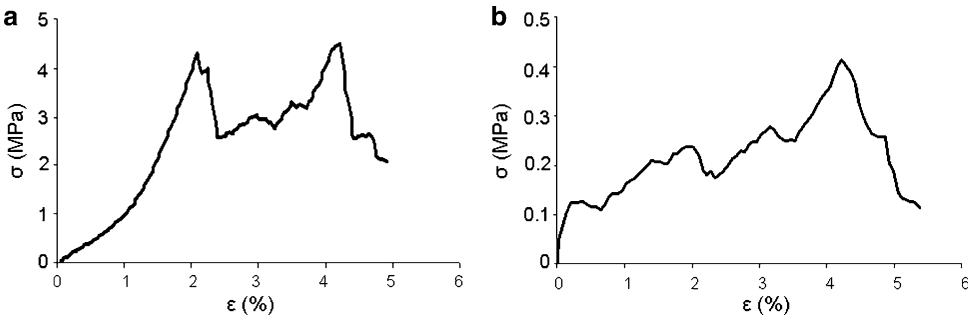

Fig. 9 Stress–strain curves typical for **a** GC-CEL2 and **b** GC-ICEL2 scaffolds

Table 5 Scaffolds mechanical strength

Scaffold material	σ_f (MPa)
GC-CEL2	5.2 ± 2.0
GC-ICEL2	0.4 ± 0.2

Five scaffolds tested for each series

glasses, were produced via sponge replication method. All samples exhibited structure, morphology and pores features (amount, size and shape) analogous to those of cancellous bone. The strength of the silica-based glass–ceramic scaffolds is comparable to that of natural bone, whereas the strength of the phosphate glass–ceramic scaffolds is one order of magnitude lower. The scaffolds showed a quite different in vitro behaviour. The silicate glass-derived scaffolds exhibited highly bioactive properties, as a hydroxyapatite layer grew on their surface after soaking in SBF. On the contrary, the phosphate scaffolds, being resorbable, underwent a dissolution process.

Therefore, the proposed scaffolds are interesting for applications in bone tissue engineering as not only their

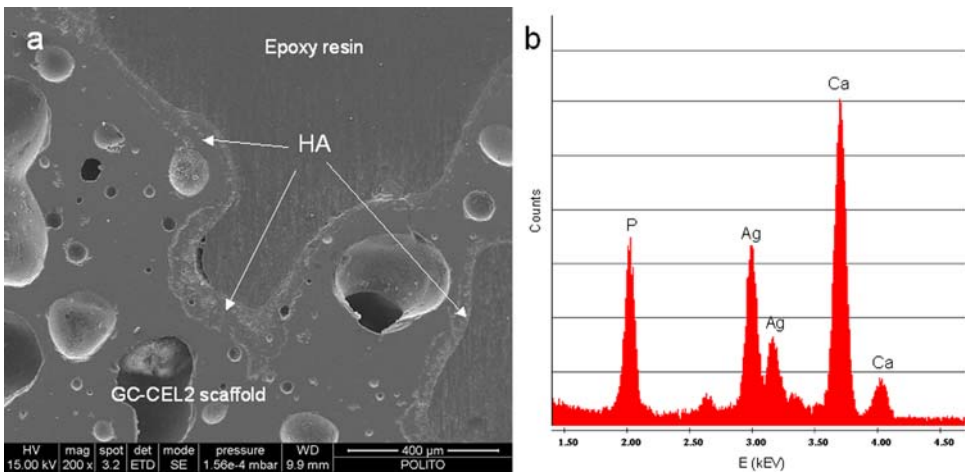

Fig. 10 In vitro tests on GC-CEL2 scaffold after 7 days in SBF: **a** scaffold cross-section and **b** EDS pattern of the newly formed phase (HA)

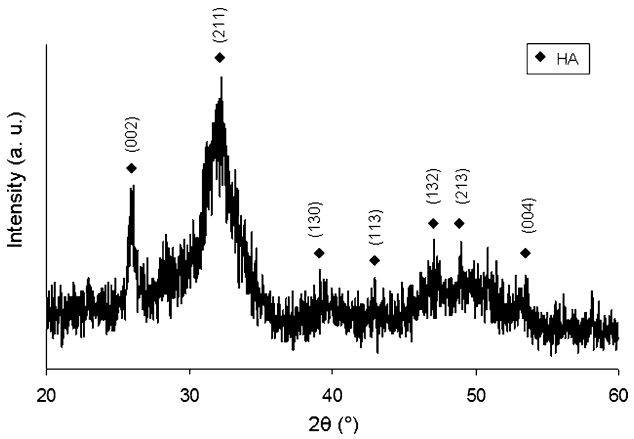

Fig. 11 XRD on GC-CEL2 scaffold after soaking for 7 days in SBF

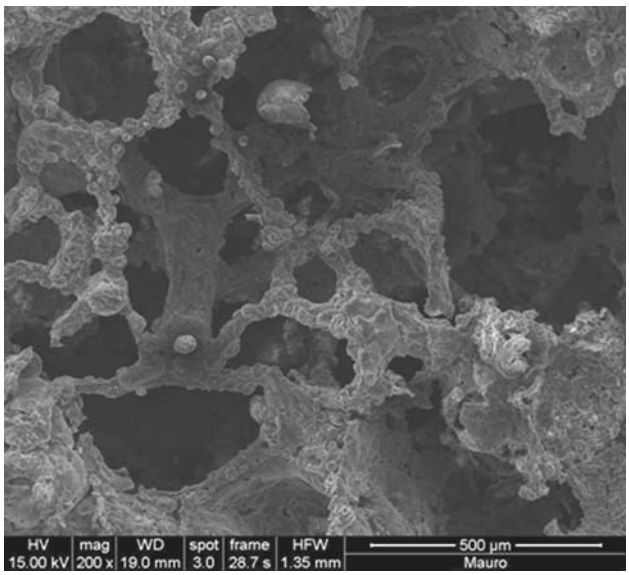

Fig. 12 Micrography of GC-ICEL2 scaffold after 30 days in SBF

shape and size, but also their structure, strength and bioactive/bioresorption can be tailored to surgical needs.

Acknowledgements The authors gratefully acknowledge Regione Piemonte (Ricerca Sanitaria Finalizzata 2008) that funded this research work.

References

1. Hulbert SF, Hench LL, Forbes D, Bowman LS. History of bioceramics. Ceram Int. 1982;8:131–40.
2. Hench LL. Bioceramics and the origin of life. J Biomed Mater Res. 1989;23:685–703.
3. Hench LL. Bioceramics. J Am Ceram Soc. 1998;81:1705–28.
4. Schlickewei W, Schlickewei S. The use of bone substitutes in the treatment of bone defects – The clinical view and history. Macromol Symp. 2007;253:10–23.
5. Ozawa N, Negami S, Odaka T, Morii T, Koshino T. Histological observations on tissue reaction of the rat calcaneal tendon to sintered hydroxyapatite. J Mater Sci Lett. 1989;8:869–71.
6. LeGeros RZ. Biodegradation and bioresorption of calcium phosphate ceramics. Clin Mater. 1993;14:65–88.
7. LeGeros RZ, Lin S, Rohanizadeh R, Mijares D, LeGeros JP. Biphasic calcium phosphate bioceramics: preparation, properties and applications. J Mater Sci: Mater Med. 2003;14:201–9.
8. Thomson RC, Yaszemski MJ, Powers JM, Mikos AG. Hydroxyapatite fiber reinforced poly(a-hydroxy ester) foams for bone regeneration. Biomaterials. 1998;19:1935–43.
9. Xigeng M, Tan DM, Jian L, Yin X, Crawford R. Mechanical and biological properties of hydroxyapatite/tricalcium phosphate scaffolds coated with poly(lactic-co-glycolic acid). Acta Biomater. 2008;4:638–45.
10. Hvid I, Jensen NC, Bunger C, Solund K, Djurhuus JC. Bone mineral assay: its relation to the mechanical strength of cancellous bone. Eng Med. 1985;14:79–83.
11. Keaveny TM, Wachtel EF, Guo XE, Hayes WC. Mechanical behavior of damaged trabecular bone. J Biomech. 1994;27:1309–18.
12. Hench LL. The story of Bioglass®. J Mater Sci: Mater Med. 2006;17:967–78.
13. Hench LL, Splinter RJ, Allen WC, Greenlee TK. Bonding mechanism at the interface of the ceramic prosthetic materials. J Biomed Mater Res. 1972;5:117–41.
14. Hench LL, Wilson J. An Introduction to Bioceramics. Singapore: World Scientific; 1993.
15. Hench LL. Bioactive materials, the potential for tissue regeneration. J Biomed Mater Res. 1998;41:511–8.
16. Hench LL, West JK. The sol–gel process. Chem Rev. 1990;90:33–72.
17. Pereira MM, Clark AE, Hench LL. Calcium phosphate formation on sol-gel-derived bioactive glasses in vitro. J Biomed Mater Res. 1994;28:693–9.
18. Sepulveda P, Jones JR, Hench LL. Characterization of melt-derived 45S5 and sol–gel-derived 58S bioactive glasses. J Biomed Mater Res. 2001;58:734–40.
19. Ahmed I, Collins CA, Lewis MP, Olsen I, Knowles JC. Processing, characterisation and biocompatibility of iron-phosphate glass fibres for tissue engineering. Biomaterials. 2004;25:3223–32.
20. Abou Neel EA, Knowles JC. Physical and biocompatibility studies of novel titanium dioxide doped phosphate-based glasses for bone tissue engineering applications. J Mater Sci: Mater Med. 2008;19:377–86.
21. Salih V, Patel A, Knowles JC. Zinc-containing phosphate-based glasses for tissue engineering. Biomed Mater. 2007;2:11–20.
22. Uo M, Mizuno M, Kuboki Y, Makishima A, Watari F. Properties and cytotoxicity of water soluble Na_2O–CaO–P_2O_5 glasses. Biomaterials. 1998;19:2277–84.
23. Bitar M, Salih V, Mudera V, Knowles JC, Lewis MP. Soluble phosphate glasses: in vitro studies using human cells of hard and soft tissue origin. Biomaterials. 2004;25:2283–92.
24. Hutmacher DW. Polymeric scaffolds in tissue engineering bone and cartilage. Biomaterials. 2000;21:2529–43.
25. Vitale-Brovarone C, Verné E, Robiglio L, Appendino P, Bassi F, Martinasso G, et al. Development of glass-ceramic scaffolds for bone tissue engineering: characterisation, proliferation of human osteoblasts and nodule formation. Acta Biomater. 2007;3:199–208.
26. Vitale-Brovarone C, Miola M, Balagna C, Verné E. 3D-glass-ceramic scaffolds with antibacterial properties for bone grafting. Chem Eng J. 2007;137:129–36.
27. Vitale-Brovarone C, Baino F, Verné E. High strength bioactive glass-ceramic scaffolds for bone regeneration. J Mater Sci: Mater Med. 2009;20:643–53.
28. Vitale-Brovarone C, Verné E, Robiglio L, Martinasso G, Canuto RA, Muzio G. Biocompatible glass-ceramic materials for bone substitution. J Mater Sci: Mater Med. 2008;19:471–8.

29. Vitale-Brovarone C, Bretcanu O, Verné E. Synthesis and characterization of a degradable phosphate glass and its use to produce resorbable scaffolds for bone substitution. J Mater Sci: Mater Med. (2009) (submitted).
30. Kokubo T, Takadama H. How useful is SBF inpredicting in vivo bone bioactivity. Biomaterials. 2006;27:2907–15.
31. Hench LL, Wilson J. Surface-active biomaterials. Science. 1984;226:630–6.
32. Hench LL. Bioceramics: from concept to clinic. J Am Ceram Soc. 1991;74:1487–1510.
33. Rizkalla AS, Jones DW, Clarke DB, Hall GC. Crystallization of experimental bioactive glass compositions. J Biomed Mater Res. 1996;32:119–24.
34. Kitsugi T, Yamamuro T, Nakamura T, Kotani S, Kokubo T, Takeuchi H. Four calcium phosphate ceramics as bone substitutes for non-weight-bearing. Biomaterials. 1993;14:216–24.
35. Radin SR, Ducheyne P. Effect of bioactive ceramic composition and structure on in vitro behavior. III. Porous versus dense ceramics. J Biomed Mater Res. 1994;28:1303–9.
36. Cao W, Hench LL. Bioactive materials. Ceram Int. 1996;22:493–507.
37. Vitale-Brovarone C, Baino F, Verné E. Feasibility and tailoring of bioactive glass–ceramic scaffolds with gradient of porosity for bone grafting. J Biomater Appl 2009; doi: 10.1177/0885328208104857.
38. Chen QZ, Thompson ID, Boccaccini AR. 45S5 Bioglass®-derived glass-ceramic scaffolds for bone tissue engineering. Biomaterials. 2006;27:2414–25.
39. Vitale-Brovarone C, Verné E, Appendino P. Macroporous bioactive glass-ceramic scaffolds for tissue engineering. J Mater Sci: Mater Med. 2006;17:1069–78.
40. Schwartz Z, Boyan BD. Underlying mechanisms at the bone-biomaterial interface. J Cell Biochem. 1994;56:340–7.